JOHN R. APEL, DONALD R. THOMPSON, DAVID G. TILLEY, and PETER VAN DYKE

HYDRODYNAMICS AND RADAR SIGNATURES OF INTERNAL SOLITONS IN THE ANDAMAN SEA

Large internal solitary waves have been observed at several locations in the Andaman Sea. Using satellite imagery and historical temperature profiles in combination with hydrodynamic and electromagnetic models, it is possible to deduce the surface and subsurface flowfield and to reproduce their surface L-band synthetic aperture radar signatures in a quantitative way.

INTRODUCTION

The Andaman Sea is located along the eastern side of the Indian Ocean between the Malay Peninsula and the Andaman and Nicobar Islands. It is a maritime regime containing internal solitary waves of extraordinary amplitude, wavelength, and speed that exhibit signatures via surface roughness variations that are visible to the eye, to cameras, to scanning imagers, and to imaging radars. Internal solitary waves, or solitons, are generally waves of depression, more or less isolated from their fellows, that propagate over great distances with very little change in shape. They have been discussed in the *Johns Hopkins APL Technical Digest*[1] in an earlier article on solitons in the Philippines.

The first scientific report of such large waves in the Andaman appears to have come from Perry and Schimke,[2] who made bathythermograph observations of an 80-meter-amplitude internal wave that had audible, breaking surface waves accompanying it. Later, Osborne et al.[3] and Osborne and Burch[4] carried out current-meter measurements on several packets of internal waves that had amplitudes up to 100 meters and current speeds in excess of 1 meter per second and established their soliton-like character. Significant modulation of the overlying surface wave spectrum accompanied these solitons, whose currents and buoyancies were large enough to disrupt and seriously damage drill ship operations in the region.

Several satellite images have also revealed that the Andaman Sea is rich in such excitations. The joint US-USSR space mission, Apollo-Soyuz, returned color photographs that showed narrow stripes of rough water in the sun glint region; one such photograph (Fig. 1) shows four packets of narrow, elongated stripes near the region of Puket. These were interpreted by Apel[5] as surface signatures of large internal waves presumably produced by semidiurnal tidal flow over underwater topography; the inferred group speeds were approximately 2.5 meters per second, as derived from their interpacket separation. In addition, examinations of visible wavelength imagery from the scanner on the Defense Meteorological Satellite Program (DMSP) spacecraft revealed similar surface signatures on several dates. DMSP data are archived at the University of Wisconsin Space Sciences and Engineering Center. Synthetic aperture radar images from the Shuttle Imaging Radar-A (SIR-A) flight on November 11, 1981, also contain several internal wave packets in the vicinity of the Andaman and Nicobar Islands.[6,7] Figure 2 sum-

Figure 1—Photograph from the US-USSR space mission Apollo-Soyuz, showing four packets of large internal solitary waves in the Andaman Sea in the eastern Indian Ocean. (Photograph courtesy of NASA.)

marizes the observations from both the in situ and satellite programs via a map showing the wave locations and patterns.

The SIR-A image is a high-resolution (40-meter resolution element), geographically corrected representation of the surface wave roughness variations; it has been selected for further analysis because of the qualities that the internal waves possess. The objectives of the analysis are (a) to use the historical density data in conjunction with the known nonlinear properties of internal solitons to estimate the amplitudes, currents, strain rates, and propagation speeds from the SIR-A image, (b) to estimate wind speed and direction from the image, and (c) to apply theories of radar backscatter modulation to the deduced hydrodynamic and wind properties, in order to calculate the radar signatures. The signatures will then be compared with image intensity modulations, and the backscatter estimates will be compared with the data.

HYDRODYNAMIC PROPERTIES

Figure 3 is a section of the SIR-A radar image of November 11, 1981, having dimensions of 51.2 by 51.2 kilometers, with the white marks along the lower border being 1-second time tics (or a distance of 7.14 kilometers). North is along the direction shown, at an angle of approximately 38 degrees from the lower edge. The internal solitons are revealed mostly by dark (smooth) regions, with the associated rough regions not clearly visible, probably due to the large, 43-degree earth-incidence angle of the synthetic aperture radar. The approximately semicircular dark region near right center is thought to be an area of rainfall toward which the local winds are blowing, as revealed by subtle windrow streaks overlying portions of the waves; the wind direction is nearly from the west. The wind speed is estimated to be about 3 to 4 meters per second, based on the general level of backscatter and the visibility of the waves, but the error in this estimate is easily ±100 percent.

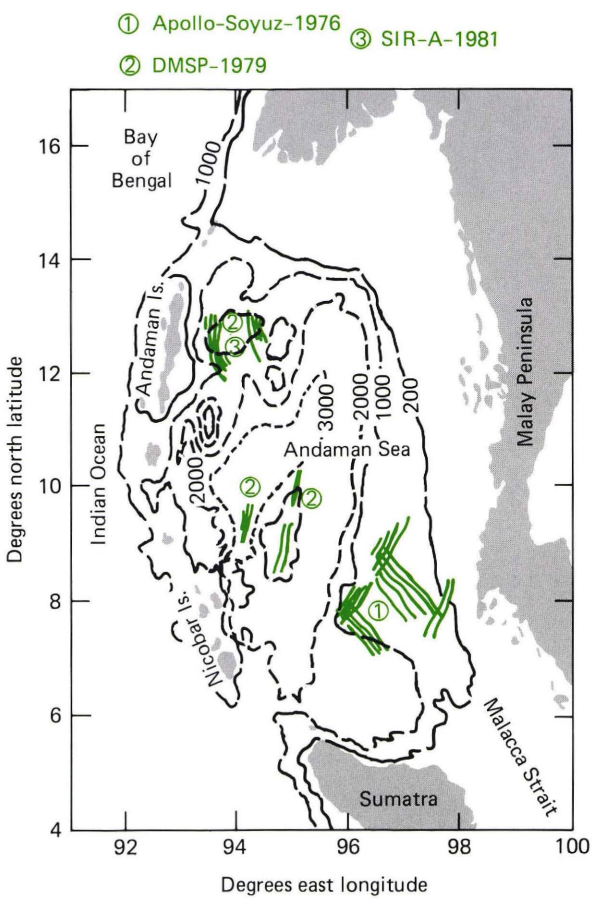

Figure 2—Bathymetric chart of the Andaman Sea illustrating known locations of internal solitary wave activity. Locations of data annotated to line drawing interpretations.

The hydrodynamic properties are estimated from the image and from the historical density data by the application of a "modulated cnoidal wave" model of the solitary waves.[8] The nonlinear characteristics of similar-appearing solitons in the Sulu Sea in the Philippines have been established experimentally,[9,10] and it was shown that the steady-state properties of each solitary wave in a packet are satisfactorily described by the Joseph solution to the generalization of the Korteweg-deVries (K-dV) shallow water equation.[11] Here we use the K-dV equation for simplicity since the more accurate Joseph solution is considered unnecessary for the purpose of estimation.

In the K-dV equation, a Mode-1 solitary wave train can be written as the product of an eigenfunction, $W(z)$, describing the relative amplitude variation with depth, z, and a horizontal amplitude function, $A(s,t)$, describing propagation along a horizontal arc, $s(x,y)$, in the x,y plane. Thus, we write for the amplitude, η,

$$\eta(x,y,z,t) = W(z)\, A(x,y,t) \,. \tag{1}$$

The equations obeyed by the separation functions W and A are

$$\frac{d^2W}{dz^2} + k_\ell^2 \left[\frac{N^2(z)}{\omega^2} - 1\right] W = 0 \,,$$

$$W(0) = W(-H) = 0 \,, \tag{2}$$

(where the ocean bottom is at the depth $-H$), and the K-dV equation,

$$\frac{\partial A}{\partial t} + c_0 \left(\frac{\partial A}{\partial s} + \gamma \frac{\partial^3 A}{\partial s^3} + \alpha A \frac{\partial A}{\partial s}\right) = 0 \,. \tag{3}$$

Here, $\omega = \omega(k_\ell)$ is the dispersion equation relating wave angular frequency, ω, to linear wave number, k_ℓ; the quantities N, γ, and α are environmental parameters termed the Brunt-Väisälä (or buoyancy) frequency, the dispersion coefficient, and the nonlinear coefficient, respectively. These may all be calculated from a knowledge of the variation of density with depth.

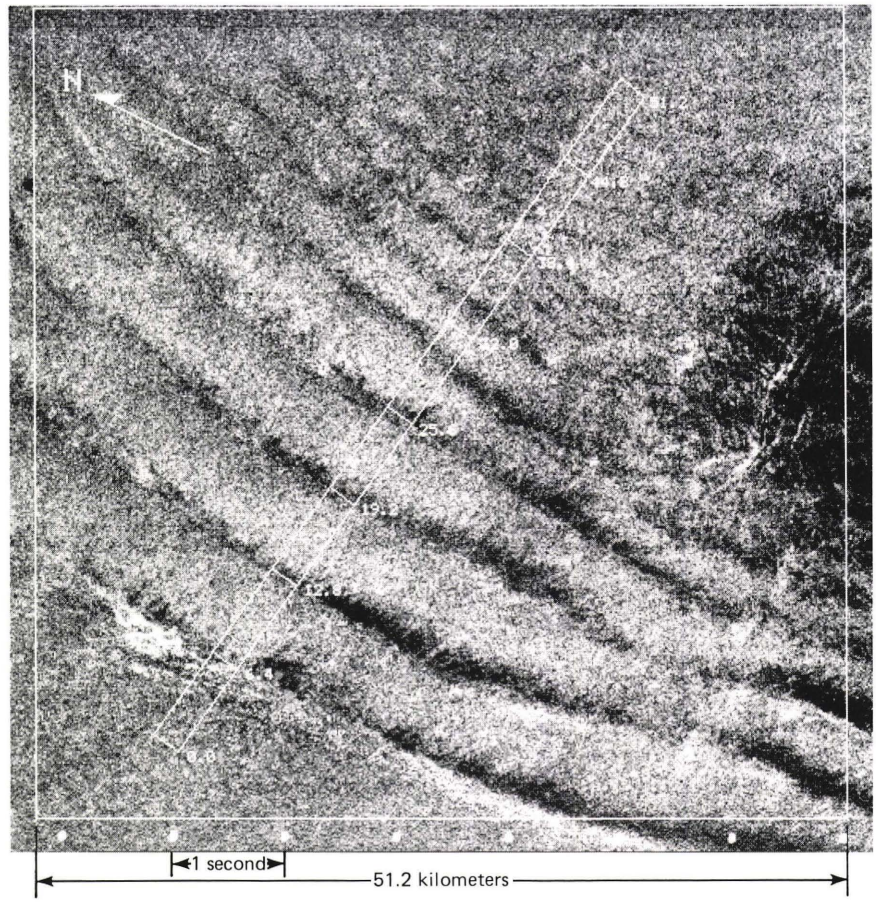

Figure 3—L-band radar image from SIR-A taken November 11, 1981, near the Andaman Islands, showing a packet of 6-kilometer-long solitons and what is thought to be a rain squall. Dimensions are 51.2 by 51.2 kilometers. (Photograph courtesy of the Jet Propulsion Laboratory.)

Known solutions to the K-dV equation include the isolated soliton function, $\mathrm{sech}^2\,[\frac{1}{2}\,(\mathbf{k}_\ell \cdot \mathbf{s} - \omega t)]$, and the square of the periodic cnoidal Jacobian elliptic function, $cn_m^2[\frac{1}{2}\,(\mathbf{k}_\ell \cdot \mathbf{s} - \omega t)]$, which contains a nonlinear parameter, m, with $0 \le m \le 1$. The function $cn(\phi)$ is a generalization of the cosine, to which it reduces when $m = 0$, as well as the hyperbolic secant, which obtains when $m = 1$. For $m < 1$, the cnoid is an oscillating function having a "stretched wavelength" greater than $2\pi/k_\ell$.

A useful approximate solution to the K-dV equation describing a bounded wave packet may be written as a modulated cnoidal function,[8] wherein a propagating envelope function, $\eta_0(s - ct)$, moving at speed, c, is assumed to multiply the periodic cnoid, just as a modulated cosine may be used to describe a propagating linear wave packet. In this fashion, the varying amplitudes and degrees of nonlinearity existing within a group of waves (such as those in Fig. 3) may be modeled without invoking the full apparatus of inverse scattering theory[10,12] in the analysis. Algebraic relationships exist between the stretched wavelength, λ_s, and k_ℓ, m, η_0, and c, and can be used to estimate the amplitude and speed if the other quantities can be evaluated. Those relationships are

$$\lambda_s = \left(\frac{2\pi}{k_\ell}\right) \cdot \frac{K(m)}{\pi/2} = \lambda_\infty \frac{K(m)}{\pi/2}\,, \tag{4}$$

$$m = \frac{\alpha\eta_0}{\frac{1}{2}\,\gamma k_\ell^2} = \frac{\alpha\eta_0}{c - c_0}\,, \tag{5}$$

$$c \approx c_0 \left(1 - \frac{1}{2}\,\gamma k_\ell^2 + \frac{\alpha\eta_0}{3}\right) \approx c_\ell + c_0 \frac{\alpha\eta_0}{3}\,. \tag{6}$$

In Eq. 4, $\lambda_\infty = 2\pi/k_\ell$ is the small-amplitude, linear wavelength and $K(m)$ is the complete elliptic integral of the first kind, which for $m = 0$ reduces to $\pi/2$, while for $m \to 1$, $K(m) \to \infty$. In Eq. 6, the speed c is given in terms of the long-wavelength speed c_0 for which $k_\ell \approx 0$. The speed of a solitary wave is increased by the nonlinear amplitude-dependent term in Eq. 6; thus, larger solitons travel faster than smaller ones, all else being equal.

Using these quantities, the modulated cnoidal wave solution can be written as

$$\eta(x,y,z,t) = -W(z)\eta_0(s - ct) \times cn_m^2\,[\tfrac{1}{2}(\mathbf{k}_\ell \cdot \mathbf{s} - \omega t + \Phi)]\,. \tag{7}$$

To apply Eqs. 4 to 7 to the case at hand, the image of Fig. 3 is used to evaluate (a) λ_∞ from the wave-

length at the rear of the wave packet, and (b) the stretched wavelength, λ_s, from the spacings of the other waves throughout the packet. The ratio λ_s/λ_∞ is used to calculate the values of $K(m)$ and m from Eq. 4; from Eq. 5 one then derives η_0. These quantities are listed in Table 1 for the Andaman Sea waves.

Having obtained the wave amplitudes, the known hydrodynamics of the waves may be used to obtain the currents, u and w, and the horizontal strain rate, $\partial u/\partial s$, as well as the other desired properties. For the quantities of interest in the present study, one has

$$u = \frac{dW}{dz}\,\eta_0(s - ct)\,cn^2(\phi)\,, \tag{8}$$

$$\frac{\partial u}{\partial s} = \frac{dW}{dz}\,\eta_0(s - ct)\,\omega\,cn(\phi)\,sn(\phi)\,dn(\phi)\,, \tag{9}$$

where we have neglected the slow variation in space and time due to the envelope function, η_0. The functions $sn(\phi)$ and $dn(\phi)$ are also Jacobian elliptic functions.[13]

In order to evaluate the equations numerically, functional forms of $W(z)$ and its derivative are required; these are obtained via numerical solutions to Eq. 2. This in turn requires a vertical profile of $N^2(z)$ in terms of water density, ρ:

$$N^2(z) = -\frac{g}{\rho}\frac{d\rho}{dz}\,. \tag{10}$$

Figure 4 shows a temperature profile from Osborne et al.[3] for the Andaman Sea. Also shown in Fig. 4 is a profile of the normalized Mode-1 eigenfunction, $W(k_\ell,z)$, evaluated for $\lambda_\infty = 2.1$ kilometers. These numerical values have been derived by solving for the Mode-1 eigenfunctions of Eq. 2 having eigenvalues k_ℓ. The temperature profile shown in Fig. 4 has been converted to density by using temperature-salinity relationships for the area.

Table 1—Wave properties of Andaman Sea solitons.

Soliton Number	*Position, s (km)*	λ_s *(km)*	*m*	η_0 *(m)*
1	12.5	6.0	0.99798	60.3
2	18.3	5.9	0.99764	60.2
3	24.0	5.6	0.99630	60.1
4	28.8	4.7	0.98561	59.4
5	32.2	3.8	0.943	56.9
6	35.3	2.9	0.755	45.5
7	37.7	2.6	0.596	35.9
8	39.0	2.4	0.425	25.6
9	41.0	2.3	0.247	14.9
∞		2.1	0	0

λ_∞ = 2.1 kilometers
α = 1.05×10^{-2} per meter
c_0 = 1.99 meters per second
c-c_0 = 0.42 meter per second

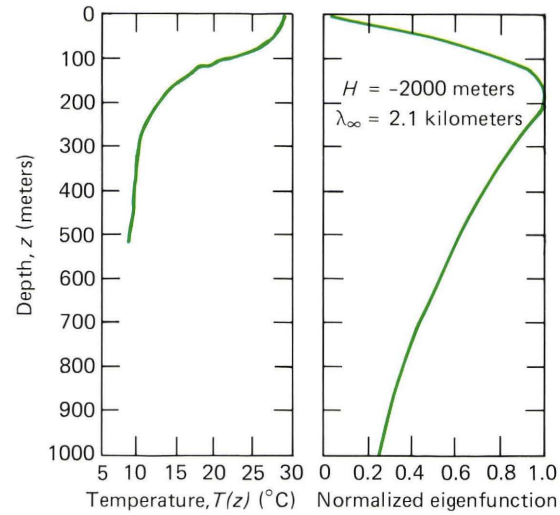

Figure 4—Vertical profiles of temperature and normalized displacement eigenfunction.

Figure 5 illustrates the phase velocity and the dispersion relationship for three values of amplitude; the amplitude increments have been obtained from the approximation of Eq. 6, while the basic dispersion relation for $\eta = 0$ comes from the numerical solution to Eq. 2. The value of k_ℓ thought to exist in the Andaman Sea wave packet is also shown in Fig. 5.

Figure 6 illustrates the estimated surface current and surface strain rates versus distance, $s - ct$, throughout approximately 40 kilometers of the packet. The peak currents are about 1.1 meters per second, the strain rates are 1.3×10^{-3} per second, and peak amplitudes (not shown) are approximately 60 meters—reasonable values in light of the measurements made in the Andaman to date.[2,4]

SIR-A IMAGE ANALYSIS

The scene showing internal waves in the Andaman Sea was obtained as a 70-millimeter film transparency that required both geometric and radiometric rectification prior to analysis. The filmstrip was scanned with a 50-micrometer photodensitometer, providing a digital database that represented 120 kilometers along the 60-kilometer swath of the SIR-A image at 25-meter resolution. This database included a region unperturbed by internal waves or large-scale oceanographic features that was used to compute the average radiometric response of the SIR-A instrument across the swath. The entire digital image was then reduced to 50-meter resolution by pixel averaging accompanied by removal of the radiometric variation across the swath with division by a fifth-order polynomial. Coefficients for the polynomial were computed by linear regression from the unperturbed segment of ocean data. Geometric rectification was accomplished by resampling the database to convert from a slant range perspective to a ground range projection across the swath. The image resolution was also reduced to 100 meters per pixel with a bilinear interpolating algorithm during this resampling

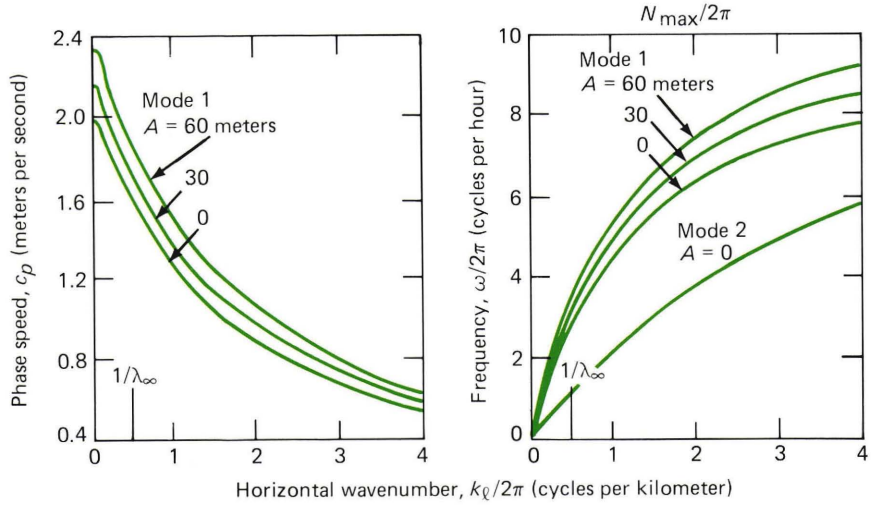

Figure 5—Phase speeds and dispersion relations of solitons of varying amplitudes.

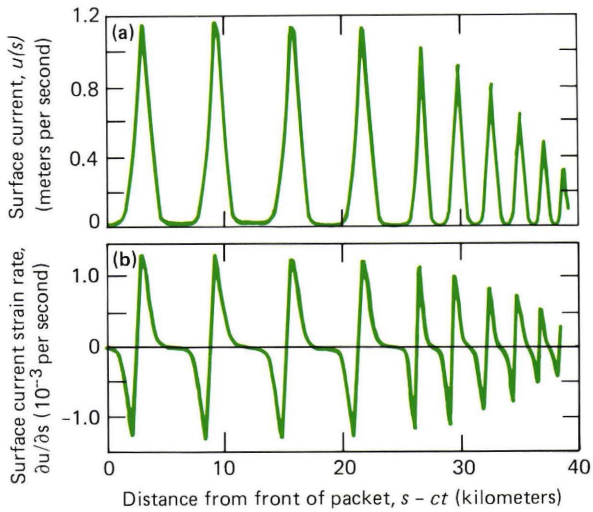

Figure 6—(a) Calculated horizontal surface currents and (b) surface strain rates for cnoidal wave packet. The front of the packet is at left.

process. Finally, the 512 × 512 pixel image shown in Fig. 3 was selected for analysis and was displayed as the square of the amplitude to represent the L-band radar cross-section variations.

The squared amplitudes were used for statistical analysis of the internal waves in the ocean scene. The first frame of Fig. 7 shows a two-dimensional Fourier transform of the 51.2-kilometer-square segment of the digital image containing the solitons that provides the range and azimuth components of the wave vector (k_r, k_a) of the surface signature. It shows the fast Fourier transform power spectrum contoured in units of one-tenth of the maximum spectral intensity over a wavenumber domain extending from $\mathbf{k} = \mathbf{0}$ at the center to $|\mathbf{k}| = 0.3125$ cycle per kilometer, or one-sixteenth of the Nyquist wavenumber, at the outermost circle. Spectral smoothing has been achieved by interpolating the fast Fourier transform database to eight times its inherent resolution of 0.0098 cycle per kilometer. One sees that the waves constitute a somewhat broadband process with a spread in angle, measured by the full width at half angle, $(\Delta\theta)_{1/2} = 30°$, and a fractional spread in wavenumber of about 100 percent.

The second spectral analysis is shown in Figs. 7b through 7d. In 7b, a profile of wave intensity along the rectangular sector shown in Fig. 3 has been computed as an average over the narrow dimension of approximately 2 kilometers and the result squared. The resultant intensity modulation across the internal wave packet has a maximum of 30 to 40 percent about the mean, and this modulation can be compared directly with the backscatter calculations ahead. The one-dimensional power and phase spectra computed from the internal wave profile are shown in Fig. 7c and 7d, respectively. The power spectrum peaks at approximately the longest wavelengths measurable in the SIR-A scene but has significantly higher wavenumber content including at least one harmonic. The phase spectrum, while noisy (black curve), shows some regularity after smoothing (white curve) with a five-point convolution filter, reducing the spectral resolution to approximately 0.05 cycle per kilometer.

SURFACE ROUGHNESS AND RADAR BACKSCATTER

The horizontal current field and current strain rate estimated using the techniques discussed above have been input into the wave-current interaction model described in the article by Thompson in this issue in order to compute the intensity modulation across the cut through the SIR-A image as shown in Fig. 3. The calculations were performed in a manner similar to that described in the Thompson article. In particular, the Bragg k-value for the SIR-A radar and imaging geometry is $k_r = 48$ per meter, which corresponds to a Bragg wavelength of about 13 centimeters. The look direction was at an angle of 30 degrees with respect to the direction of propagation of the internal wave feature.

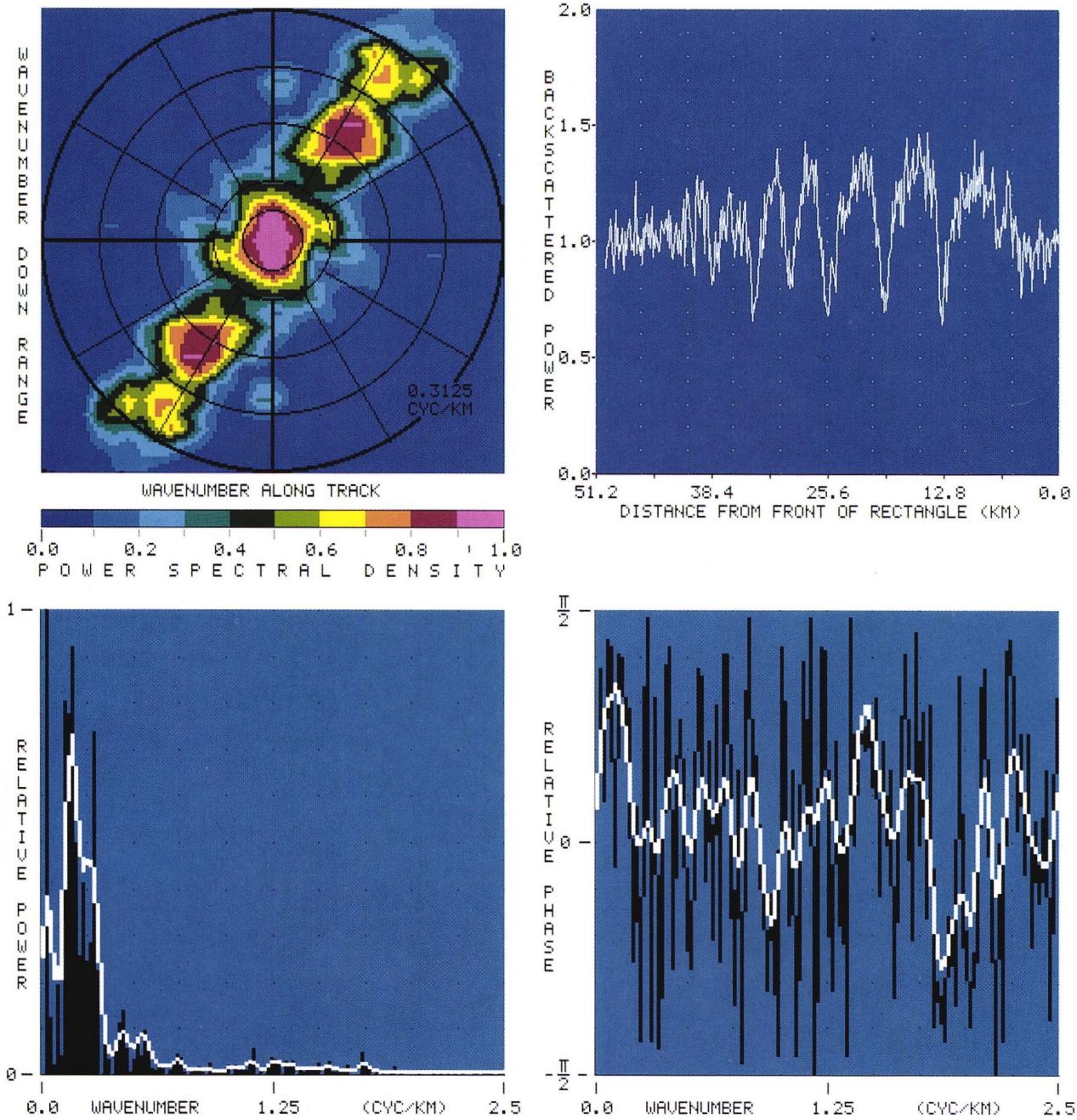

Figure 7—Top left (7a): two-dimensional fast Fourier transform computed from the 51.2-kilometer square of Fig. 3, showing the relative power as a function of wavenumber in the wave surface signature, contoured in units of one-tenth maximum power. Top right (7b): intensity modulation across the internal wave packet as computed within the rectangle shown in Fig. 3. Bottom left (7c): unit normalized power spectrum for the spatial series of 512 samples representing the modulation profile for the internal wave packet. Bottom right (7d): the phase spectrum for the internal wave profile with a maximum wavenumber equal to one-half the Nyquist limit.

Figure 8 shows a comparison between the measured intensity modulation along the cut through the SIR-A image of Fig. 3 (colored curve) and the predicted modulation from our wave-current interaction model (black curve). One can see from Fig. 8 that the predicted modulation depth agrees fairly well with that measured from the synthetic aperture radar image. Although the intensity minima occur at nearly the same position, the spatial behavior of the predicted and measured curves is rather different. In previous wave-current interaction calculations, where the surface-current features were obtained from direct ground-truth measurements (e.g., Ref. 14), a comparison of the spatial behavior of the measured and predicted modulation has normally shown close agreement, for example, to within factors of 2 to 3. It is therefore not clear at this time why such agreement is not seen in the present study. One possible explanation could be the importance of the modu-

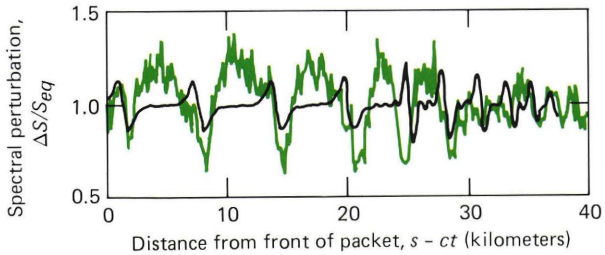

Figure 8—Comparison of observed (colored curve) and calculated (black curve) radar backscatter power modulation from rectangle of Fig. 3. The phase of the calculated modulation is reproduced quite well, but the amplitudes are generally underestimated by factors of 2 or more. The overall agreement is considered reasonable.

lation of the longer waves as discussed by Thompson. Also, it may be seen from Fig. 3 that the wave packet is not really a plane wave but is, in fact, a cylindrical wave emanating from a source beyond the upper right corner of the image. In the present calculation, a one-dimensional current field is assumed, and the omission of the transverse components of the surface-current field could be the cause of some disagreement in our comparison.

Other possible sources of discrepancy can be in the estimates of currents and wind speeds, in the variation in antenna pattern along the wave train, and in the large incidence angle of the SIR-A radar.

SUMMARY AND CONCLUSIONS

It is the central result of this paper that the current theory for internal solitary waves and radar backscatter modulations from them gives reasonable estimates for both the hydrodynamics and the electromagnetics, at least for low wind speeds and 30-centimeter radar wavelengths. The cnoidal wave packet model, when used with the SIR-A imagery and a historical density profile, gives amplitudes of 60 meters, currents of 1.1 meters per second, and strain rates of 1.3×10^{-3} per second, values thought to be well within ± 50 percent of the actual ones. The theory for the rate of change of surface wave action in the relaxation time approximation is used together with the cnoidal currents and strain rates plus wind velocity estimates from the synthetic aperture radar image to calculate backscatter modulation, and the results are compared with image intensity modulations. We obtain agreement in the depths of modulation to within a factor of 2, with the theory generally yielding no more than a 50 percent underestimate. Similar results have been obtained in two field experiments where both in situ and synthetic aperture radar data were available. It is felt, therefore, that the methods presented here imply a reasonably quantitative understanding of the basic hydrodynamic and electromagnetic processes at work, within the range of environmental and radar parameters encountered in the study.

REFERENCES

1. J. R. Apel and J. R. Holbrook, "Internal Solitary Waves in the Sulu Sea," *Johns Hopkins APL Tech. Dig.* **4**, 267-275 (1983).
2. R. B. Perry and G. R. Schimke, "Large Amplitude Internal Waves Observed Off the Northwest Coast of Sumatra," *J. Geophys. Res.* **70**, 2319-2324 (1965).
3. A. R. Osborne, T. L. Burch, and R. I. Scarlet, "The Influence of Internal Waves on Deep-Water Drilling," *J. Petroleum Tech.*, 1497 (1978).
4. A. R. Osborne and T. L. Burch, "Internal Solitons in the Andaman Sea," *Science* **208**, 451 (1980).
5. J. R. Apel, "Observations of Internal Wave Surface Signatures in ASTP Photographs," *Apollo-Soyuz Test Project* **II**, F. El-Baz and D. M. Warner, eds., NASA SP-412 (1979).
6. J. B. Cimino and C. Elachi, *Shuttle Imaging Radar-A (SIR-A) Experiment*, NASA/JPL 82-77, pp. 5-53 (1982).
7. J. P. Ford, J. B. Cimino, and C. Elachi, *Space Shuttle Columbia Views the World with Imaging Radar: The SIR-A Experiment*, NASA/JPL 82-95, pp. 144-145 (1983).
8. J. R. Apel and F. I. Gonzales, "Nonlinear Features of Internal Waves off Baja California as Observed from the Seasat Imaging Radar," *J. Geophys. Res.* **88**, 4459-4466 (1983).
9. J. R. Apel, J. R. Holbrook, A. K. Liu, and J. J. Tsai, "The Sulu Sea Internal Soliton Experiment," *J. Phys. Oceanogr.* **15** (to be published, 1985).
10. A. K. Liu, J. R. Holbrook, and J. R. Apel, "Nonlinear Internal Wave Evolution in the Sulu Sea," *J. Phys. Oceanogr.* **15** (to be published, 1985).
11. R. I. Joseph, "Solitary Waves in a Finite Depth Fluid," *J. Phys. A: Math. Gen.* **10**, L225-L227 (1977).
12. T. Kuboto, D. R. S. Ko, and L. Dobbs, "Propagation of Weakly Nonlinear Internal Waves in a Stratified Fluid of Finite Depth," *J. Hydronaut.* **12**, 157-165 (1978).
13. A. Abramowitz and I. A. Stegun, eds., *Handbook of Mathematical Functions*, U.S. Government Printing Office, Washington, p. 567 (1965).
14. R. F. Gasparovic et al., *SARSEX Interim Report*, JHU/APL STD-R-1200 (1985).

ACKNOWLEDGMENTS—The authors appreciate the data support by NASA's Johnson Space Center and the provision of SIR-A imagery by Charles Elachi of the Jet Propulsion Laboratory.

THE AUTHORS

JOHN R. APEL (center) is a physicist/oceanographer and the Chief Scientist of the Milton S. Eisenhower Research Center. His interest in oceanic internal waves dates from 1973 observations of their surface signatures in Landsat imagery, and that interest has developed into a decade-long research program that continues today. Dr. Apel holds degrees in physics and mathematics from the University of Maryland, has a Ph.D. in applied physics from The Johns Hopkins University, and has published extensively in plasma physics and oceanography. He has directed two government laboratories and is the receipient of several federal awards, including a U.S. Commerce Department gold medal for work on the ocean-viewing spacecraft, Seasat. He has held faculty appointments at the Universities of Miami and Washington, is currently lecturing in physical oceanography at the Whiting School of Engineering at The Johns Hopkins University, and is writing a graduate-level textbook on principles of ocean physics.

DONALD R. THOMPSON's biography can be found on p. 353.

DAVID G. TILLEY (left) was born in Binghamton, N.Y., in 1947. He received a B.S. degree in physics from The University of Virginia in 1969, received an M.S. and a Ph.D. degrees in nuclear engineering in 1973 and 1976, and the M.S.E.E. degree in 1979 from The Pennsylvania State University. His graduate research in medical imaging was continued as a post-doctoral fellow in radiology at the Milton S. Hershey Medical School during 1977. Since joining the Data Processing Branch in 1979, he has coordinated image-processing applications in oceanography, missile guidance, sonar acoustics, radiography, and aerial photography with research interests in remote sensing and the surface scattering of electromagnetic radiation. Currently, his particular focus is on the analysis of coherent speckle noise for estimating the response characteristics

of the Doppler imaging radars flown aboard the NASA space shuttles. Dr. Tilley is a senior member of IEEE, an associate member of Sigma Xi, and a charter member of The Planetary Society.

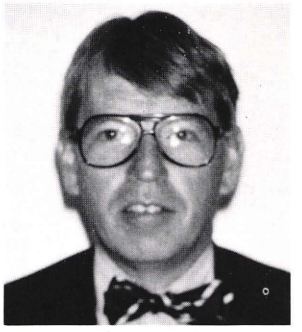

PETER VAN DYKE was a senior engineer in APL's Submarine Technology Department from 1983 to 1985, where he worked on problems relating to submarine propulsion and detection. Before that, he worked for Hydronautics, Inc., where his interests involved the development and operation of a real-time ship and submarine maneuvering and propulsion simulator, mathematical simulations of various hydrodynamic phenomena including wing tip vortex motion and blood flow, and operations research problems involving containership loading algorithms. After joining APL, his work concerned radar propagation simulation and internal wave mechanics. He earned a B.S. from Webb Institute in 1960, an S.M. and a Ph.D. from Harvard University in 1964, and an S.M. in management science from The Johns Hopkins University in 1970. In 1985, Dr. Van Dyke joined the Research Department of T. Rowe Price Associates in Baltimore, where he is now a vice president.